JOURNAL OF AGRICULTURAL AND FOOD CHEMISTRY

Microchemical Structure of Soybean Seeds Revealed in Situ by Ultraspatially Resolved Synchrotron Fourier Transformed Infrared Microspectroscopy

LUKASZ N. PIETRZAK* AND S. SHEA MILLER

Eastern Cereal and Oilseed Research Centre, Agriculture and Agri-Food Canada, Ottawa, Ontario K1A 0C6, Canada

The distribution of water in soybean seeds during imbibition varies with the chemical composition of the tissue. To understand the dynamics of imbibition, the proteins, lipids, and carbohydrates of the cotyledons and hilum region in mature soybean seeds were mapped using synchrotron Fourier transformed infrared microspectroscopy, based on characteristic peaks for each component: amide I at 1650 cm^{-1} and amide II at 1550 cm^{-1} for protein, lipid ester stretch at 1545 cm^{-1}, and the region from 1200 to 900 cm^{-1} for carbohydrates. The amount and configuration of the proteins varied across the cotyledon, as well as the amount of lipid and carbohydrate. It was found that protein distribution across the cotyledon is similar to water distribution during imbibition. The chemistry of the hilum region was also studied, as this is the point of water entry, and differences in the chemical composition of the tissues studied were observed.

KEYWORDS: FTIR microspectroscopy; synchrotron; chemical mapping; soybean

INTRODUCTION

The soybean, *Glycine max* (L.) Merr., is an important cash crop in Ontario, Canada. Soybeans are used for oil and protein production, as well as for both traditional Oriental food products such as tofu, miso, and natto and meat (texturized vegetable protein) and dairy (soy milks and frozen desserts) replacement in conventional Western diets. For each of these uses, different types of soybean are used, with end use being based primarily on chemical composition. Virtually all soy-based food products require preliminary soaking in water to hydrate the bean. It is very important from a processor's perspective that the soaking time of the seeds is uniform. Thus, consistency in the rate and extent of imbibition is a major quality parameter.

The distribution of water in soybean seeds during imbibition varies with the chemical composition of the tissue (*1*). The embryonic axis contains 43% carbohydrates and 11% lipids, whereas the cotyledons contain about 29% carbohydrates and 23% lipids (*2*). The protein contents of both structures are similar (∼47%), but the nature of the proteins is quite different. Although Aspinall et al. (*3*) characterized the main polysaccharides of the hull and cotyledon of soybean, their procedures for removal of contaminating protein would have resulted in the loss of soluble polysaccharides as well as oligosaccharides and free sugars. Thus, due to the bulk nature of the analyses of Aspinall et al. (*3*), the nature of the carbohydrates in the various tissues, particularly the proportion of soluble and insoluble polysaccharides, has not been well-defined. Soluble polysaccharides are noted for having a high water-holding capacity, which would influence imbibition and affect the pattern of water distribution during this process.

The gross chemical composition of plant tissues can be determined using both wet chemistry and histochemistry (conventional microscopy). Chemical compounds can be localized but not precisely quantified in situ using histochemistry, but as with wet chemistry, sample preparation can be time-consuming and may introduce artifacts. In addition, neither of these methods permits in situ chemical analysis. The only available ultraspatially resolved method is Fourier transformed infrared (FTIR) microspectroscopy.

FTIR microspectroscopy is a combination of FTIR spectroscopy with microscopy. Conventional light microscopic techniques can image samples with much better contrast and spatial resolution, but cannot match the level of chemical information afforded by infrared spectroscopy. Joining the two techniques thus provides specific chemical information at defined points in the sample. Recently, to increase the signal-to-noise ratio as well as to increase the infrared (IR) energy, synchrotron radiation has been used for FTIR microspectroscopy instead of a conventional IR light source (*4*, *5*). Infrared microscopes are very much like conventional visible light microscopes, except that the optics are reflective surface mirrors instead of lenses which transmit radiation. Because of this, modern IR microscopes operate very much like typical visible light microscopes for sample viewing, with a variety of methods for enhanced sample visualization (e.g., polarized light, fluorescence illumination or differential interference contrast) (*6*−*8*).

The objective of the current work was to utilize synchrotron-powered IR microspectroscopy to chemically map the soybean

* Author to whom correspondence should be addressed [e-mail pietrzakln@agr.gc.ca; telephone (613) 759-1646; fax (613) 759-1701].

10.1021/jf050608x CCC: $30.25 Published 2005 by the American Chemical Society
Published on Web 10/29/2005

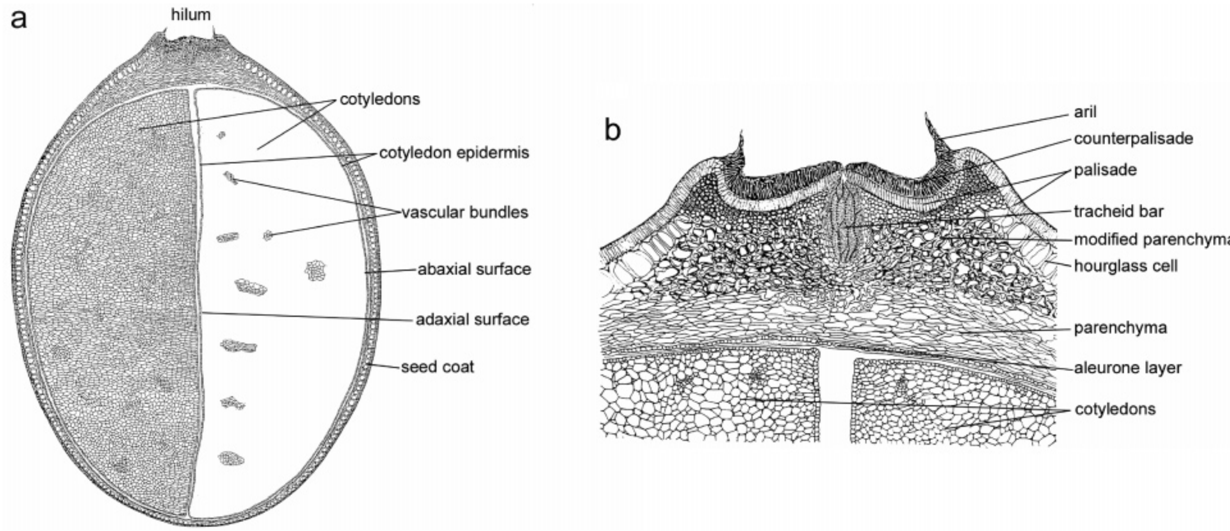

Figure 1. Diagram of (**a**) cross section of soybean seed and (**b**) cross section of hilum region.

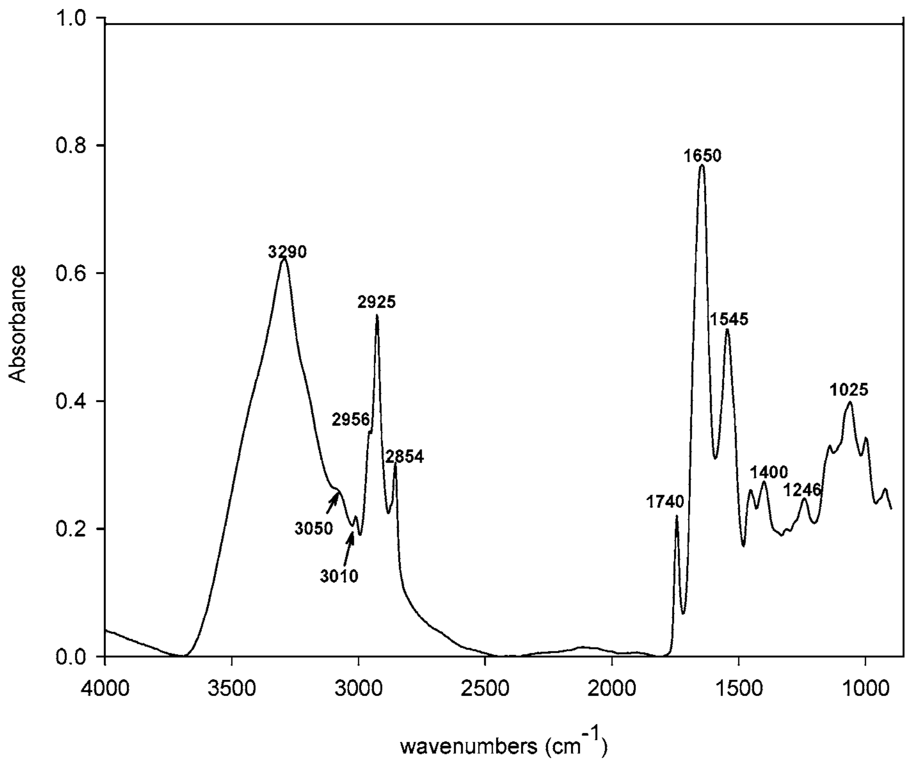

Figure 2. FTIR spectrum (4000–900 cm^{-1}) of soybean cotyledon.

seed. The cotyledon and hilum regions of the seed were the subject of our FTIR spectral investigation.

MATERIALS AND METHODS

Mature soybean seeds (cv. AC Colibri) grown at the Central Experimental Farm of Agriculture and Agri-Food Canada, Ottawa, ON, Canada, and harvested in 2002, were used in all experiments. Experiments were performed with an FTIR microspectrometer using synchrotron radiation at beam line U10b of the VUV (vacuum/ultraviolet) ring of the National Synchrotron Light Source (Brookhaven National Laboratory, Upton, NY).

Instrumentation. *Optical Configuration.* A two-mirror system (M1 and M2) collects and re-images the synchrotron infrared source at a point just outside the storage ring. The mirrors focus the beam through a wedged diamond window with an 11 mm aperture. The spectral range delivered extends from ~10 to ~40000 cm^{-1}. The infrared region is then collimated to a diameter of 14 or 8 mm and transported under rough vacuum through a KBr (or polyethylene) window and into the nitrogen-purged end station.

Table 1. Characteristic Frequencies of Common Bands Observed in Soybean Mid-IR Microspectroscopy

3290 cm^{-1}	O—H stretch (mainly proteins and carbohydrates)
3050 cm^{-1}	amide B, N—H bending, first overtone (proteins)
3010 cm^{-1}	H attached to C═C; C—H stretch (unsaturated lipids)
2925 cm^{-1}	C—H stretch (neutral lipids, proteins, and carbohydrates)
2854 cm^{-1}	C—H stretch (neutral lipids, proteins, and carbohydrates)
1740 cm^{-1}	C═O stretch (lipid ester stretch)
1650 cm^{-1}	C═O stretch (amide I, protein)
1545 cm^{-1}	N—H bending (amide II, protein)
1370 cm^{-1}	hemicelluloses
1320 cm^{-1}	hemicelluloses
1400 cm^{-1}	cellulose
1246 cm^{-1}	cellulose
1200–1000 cm^{-1}	C—H stretching, arising mainly from carbohydrates (includes both cellulosic and starch-type polysaccharides)

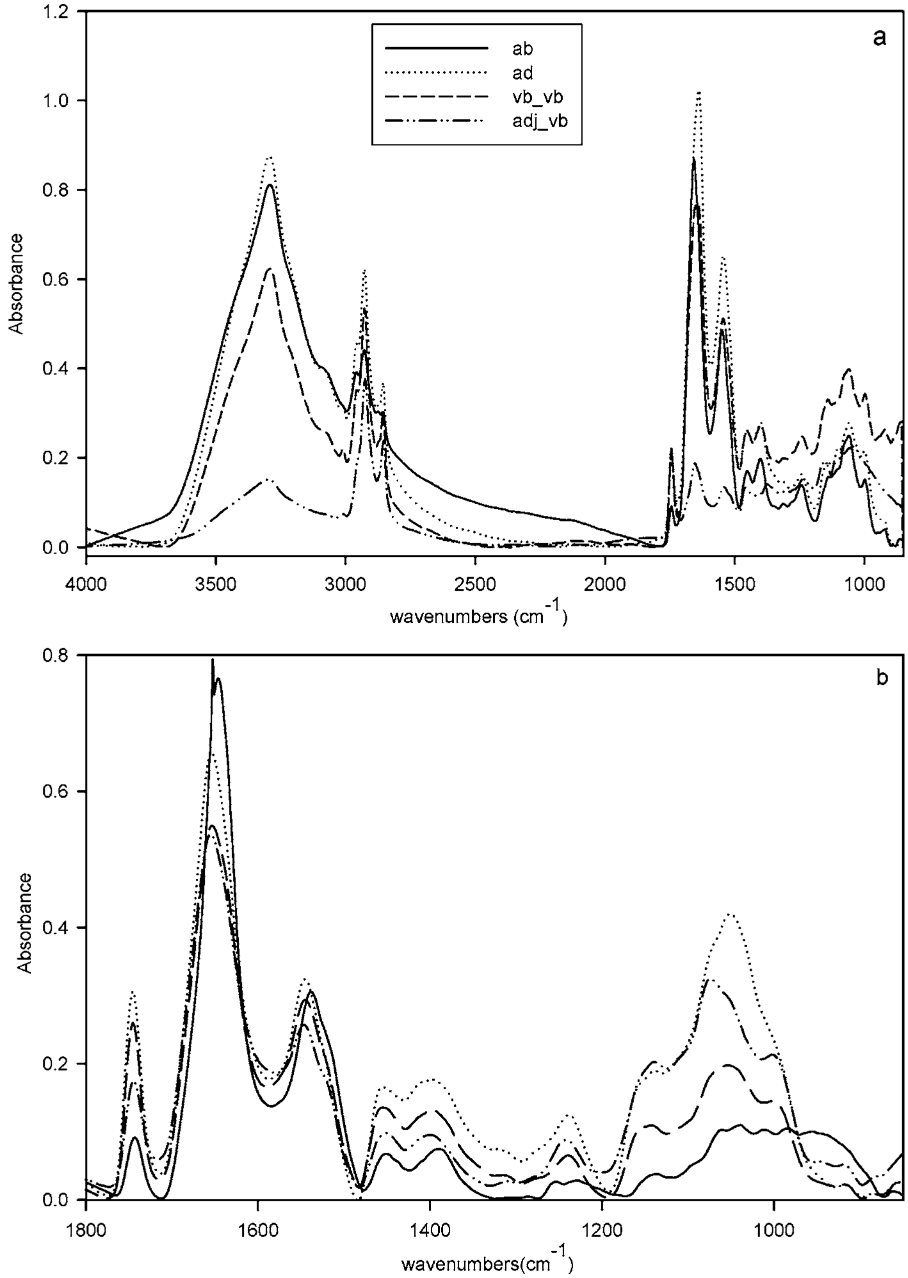

Figure 3. Spectra from different regions of cotyledon: (**a**) spectral range 4000–900 cm^{-1}; (**b**) spectral range 1800–900 cm^{-1}. ab, abaxial; vb_vb, between vascular bundles; adj_vb, adjacent to vascular bundle; ad, adaxial.

Microspectrometer. The end station at beamline U10b consists of a Magna 860 step-scan FTIR spectrometer (Thermo-Nicolet) and a Continμum IR microscope (Spectra-Tech). The Magna 860 FTIR spectrometer is fitted with CaF_2, KBr, and Si beam splitters and an internal deuterated triglycine sulfate−potassium bromide detector (DTGS-KBr). The Continμum IR microscope is equipped with a 32 × Schwarzchild IR objective, double-aperture, and a motorized X−Y scanning stage for spectral mapping with a step resolution of 1 μm and a small-area mercury−cadmium−telluride (MCT) photoconductive detector. The microscope is also equipped with two conventional (4× and 20×) objectives for sample viewing and basic focusing. The complete system is run by Nicolet Omnic E.S.P v. 6.1a software for "point and shoot" spectral collection and Atlμs software for mapping. Data analysis was performed using the same software. All spectra were subjected to baseline correction and smoothing.

Sample Preparation. For conventional sample preparation, mature, dry, untreated seeds were sectioned using either a Sorvall Porter-Blum rotary ultramicrotome equipped with glass knives or a Leica rotary microtome equipped with disposable metal blades (Feather Safety Razor Co., Osaka, Japan). Whole, dry soybeans were mounted on methacrylate stubs using epoxy resin, sectioned at 5 μm, and placed on BaF_2 windows (2 mm × 13 mm, Thermo Instruments Inc.) for transmission analysis. A drop of ethanol or methanol was placed on the surface of the window/slide, and the dry section was transferred from the microtome to the droplet. Samples for microspectroscopy were prepared from four or five seeds, and at least three samples were prepared from every investigated tissue of each seed. Spectra were taken from four areas of the cotyledon (abaxial epidermis, adjacent to vascular bundle, halfway between vascular bundles, and adaxial epidermis) and five tissues of hilum (palisade layer, counter-palisade layer, modified parenchyma and aril).

Analysis. *Microspectroscopy.* Sections were mounted on BaF_2 windows for transmission analysis. Windows in special holders were placed on the microscope stage, and 125 mid-IR spectra (4000−900 cm^{-1}) at a resolution of 4 cm^{-1} were taken at three different spots in the same tissue of the soybean seed, with the microscope in transmission mode. In general, the measuring spot (12 × 12 μm) covered about one

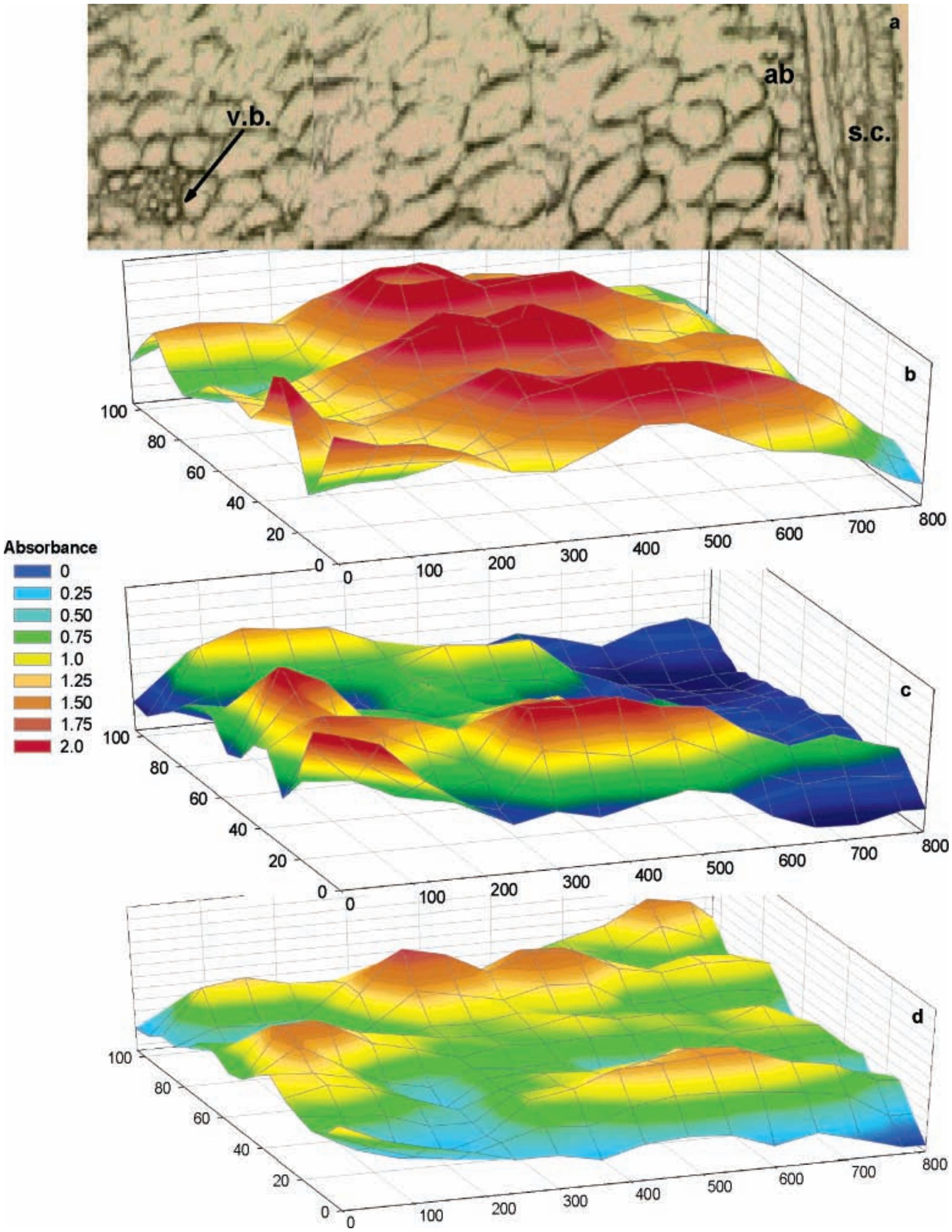

Figure 4. Pseudo 3D image of distribution of proteins, lipids, and polysaccharides in soybean seeds (**a**) bright field image of the mapped area (104 × 897 Fm) (ab, abaxial; vb, vascular bundle; sc, seed coat); (**b**) proteins (amide I at 1650 cm^{-1}); (**c**) lipids (1750 cm^{-1}); (**d**) carbohydrates (peaks at 1200–900 cm^{-1}) within cotyledon. Legend represents colors assigned to IR absorbance values.

or two cells. Reference (background) spectra were taken from a clean area of the window just outside the specimen.

All spectra and maps were evaluated using OMNIC v 6.1.1a and SigmaPlot 9.0 software. To extract information on protein secondary structure from IR spectra, we have used a Fourier self-deconvolution computational procedure. This procedure, sometimes referred to as "resolution enhancement", decreases the widths of IR bands, allowing for increased separation of overlapping component bands present under a composite band (*9*).

RESULTS AND DISCUSSION

A diagram showing a cross section of a mature soybean is presented in **Figure 1a**. The cotyledon and hilum regions were the subjects of our FTIR spectral investigation. The two cotyledons, which make up the bulk of the seed, are composed mainly of proteins, lipids, and carbohydrates (mostly cell wall polysaccharides and sugars). The soybean variety used in this study, AC Colibri, contains ∼20% protein, 41% lipid, and ∼9% soluble carbohydrates.

A typical IR absorption spectrum of a cotyledon is presented in **Figure 2**, and the representative bands shown are summarized

Table 2. Peak Areas of Lipids and Proteins in Different Regions of the Cotyledon and Ratios of Lipid to Proteins and Amide II to Amide I

		proteins		ratio	
tissue	lipids	amide I	amide II	lipids: amide I	amide II: amide I
abaxial	1.12	33.61	15.15	0.033	0.451
between VB[a]	4.33	82.31	29.07	0.053	0.353
adjacent to VB	3.71	36.31	13.38	0.102	0.368
adaxial	2.89	43.17	18.16	0.067	0.421

[a] VB, vascular bundle.

in **Table 1**. The broad band observed at 3290 cm^{-1} corresponds to O−H stretching vibrations, arising mainly from proteins and carbohydrates. In some cases (tissue dependent) a narrow band or shoulder was observed at 3050 cm^{-1} and is attributed to proteins (amide B, N−H bending, first overtone). There is also a narrow band at 3010 cm^{-1} that indicates the presence of unsaturated lipids (H attached to C=C; C−H stretch). The bands at 2925 and 2854 cm^{-1} represent C−H stretch vibrations, arising mainly from neutral lipids, proteins, and carbohydrates. The band at 1740 cm^{-1} is characteristic of ester bonds (C=O stretch) arising from lipids. In the region between 1700 and 1500 cm^{-1}, the amide I band at 1650 cm^{-1} (protein, C=O stretch) and the amide II band at 1545 cm^{-1} (protein, N−H bending) can be observed. Although small and difficult to distinguish in **Figure 2**, hemicellulosic polysaccharides are characteristically seen at about 1370 and 1320 cm^{-1}; bands at 1400 and 1246 cm^{-1} can be attributed to cellulose. The bands between 1200 and 1000 cm^{-1} represent C−H stretching vibrations arising mainly from carbohydrates.

The distribution of these compounds within the cotyledon is not uniform; FTIR spectra acquired from different regions of the cotyledon show substantial differences. Cotyledon spectra were collected from the abaxial epidermis, adjacent to the vascular bundles, halfway between the vascular bundles, and the adaxial epidermis (**Figure 3a**). Although, in general, the shapes of the spectra are similar, there are clear differences in the relative amounts of different functional groups, as reflected in the different peak sizes, particularly those of the lipid ester stretch, amide I, and amide II at 1740, 1650, and 1545 cm^{-1}, respectively, and in the carbohydrate region between 1300 and 950 cm^{-1}. The carbohydrate region includes both cellulosic and starch-type polysaccharides.

The spectra obtained show differences in absorption intensity across the whole mid-IR range. However, the peaks in the region 3700−2700 cm^{-1} are mostly multicompound in origin and cannot be assigned to one chemical type, as can the peaks in the range 1800−1000 cm^{-1}. Thus, spectra from the latter region have been expanded and are presented in **Figure 3b**. Peak areas from **Figure 3b**, which represent the relative concentrations of the lipids (at 1750 cm^{-1}) and proteins (amide I and amide II) are compiled in **Table 1**. These peak area data, and the ratios of the peak areas, indicate that the concentration of proteins and lipids varies across the cotyledon, and these differences are clearly shown in the spectral maps of the cotyledon presented in **Figure 4**.

The lipids, proteins, and carbohydrates form clusters within the cotyledon (**Figure 4**). Wetzel et al. (*10*) reported similar results in corn and wheat seeds. The highest concentration of lipids (based on the peak area at 1750 cm^{-1}) was observed in the region between and around the vascular bundles (**Figure 4c**). The peripheral areas of the cotyledon contain the lowest amount of lipids, although the adaxial side appears to have roughly twice as much as the abaxial side (**Table 2**). Miller et al. (*11*) reported a gradient in lipid concentration from the adaxial to the abaxial side of the cotyledon during soybean seed development, on the basis of histochemical data. The presence of unsaturated lipids (olefinic C−H stretch at 3010 cm^{-1}) is also detectable in the cells adjacent to vascular bundles (**Figures 3** and **4c**).

The distribution of amide I (at 1650 cm^{-1}) and amide II (at 1550 cm^{-1}), which represent protein, is different from that of lipids (**Figure 4b**). The highest concentration of proteins was observed in the cells between vascular bundles and the abaxial side of the cotyledon. The amount of protein adjacent to the vascular bundles is almost the same as in the abaxial region, but much lower than in the adaxial region. A similar protein distribution was previously reported by Wetzel et al. (*10*). The relatively high amount of protein in the central part of the cotyledon may explain the higher concentration of water in the same region during seed imbibition (*1*). Proteins, in general, are much more hydrophilic than lipids and even some polysaccharides.

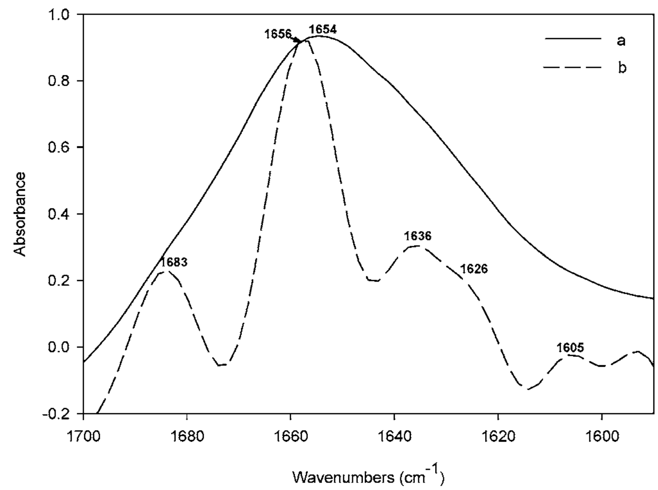

Figure 5. Spectrum (1700–1590 cm^{-1}) representing amide I from cotyledon: (**a**) original FTIR spectrum; (**b**) Fourier self-deconvolved spectrum.

Different aspects of protein tertiary and quaternary structure become visible after application of Fourier self-deconvolution within the amide I region (1700−1600 cm^{-1}). **Figure 5** shows the characteristic peaks of α-helix (1656 cm^{-1}) and/or β-sheet (1636 cm^{-1}) origin. Peaks at about 1683 and 1626 cm^{-1} are attributed to aggregated strands of antiparallel β-sheet, and the peak at 1605 cm^{-1} corresponds to side-chain vibration (*12*, *13*).

Fourier self-deconvolved spectra of amide I from different parts of the cotyledon show that protein structural conformation is also tissue dependent (**Figure 6**). Proteins associated with the abaxial region of the cotyledon contain α-helix (1656 cm^{-1}) and β-sheet (1636 cm^{-1}) features, as well as aggregated strands of antiparallel β-sheet (1683 cm^{-1}) (*14*). The proteins located between the vascular bundles have similar structural features, with an additional peak from side-chain vibration at 1610 cm^{-1}. The vascular bundle region contains proteins mostly consisting of α-helix. Although the α-helix appears shifted in this region (1646 cm^{-1}), this could be caused by water bound to proteins. Water absorbs strongly around 1645 cm^{-1} (i.e., in the region where the α-helix band occurs) and may cause an absorption shift (*12*). The adaxial region is characterized by proteins with predominantly β-sheet conformation, although other conformations are also present. Clearly, protein configuration and, thus, probably, protein composition are not uniform across the cotyledon.

The scar formed by the abscission of the mature seed from the funiculus (which connects the developing ovule and seed with the ovary) is called the hilum (*15*). This tissue is postulated to be the route for water entry into the seed upon imbibition, hence its importance from a quality standpoint (*1*, *16*). Five tissues from the hilum area were analyzed: the palisade layer, counterpalisade layer, modified parenchyma, aril, and tracheid bar (for hilum anatomy, see **Figure 1b**).

Spectra from the hilum region are presented in **Figure 7a**. The greatest spectral differences between cell types were observed in the region from 1800 to 1000 cm^{-1}, which has been

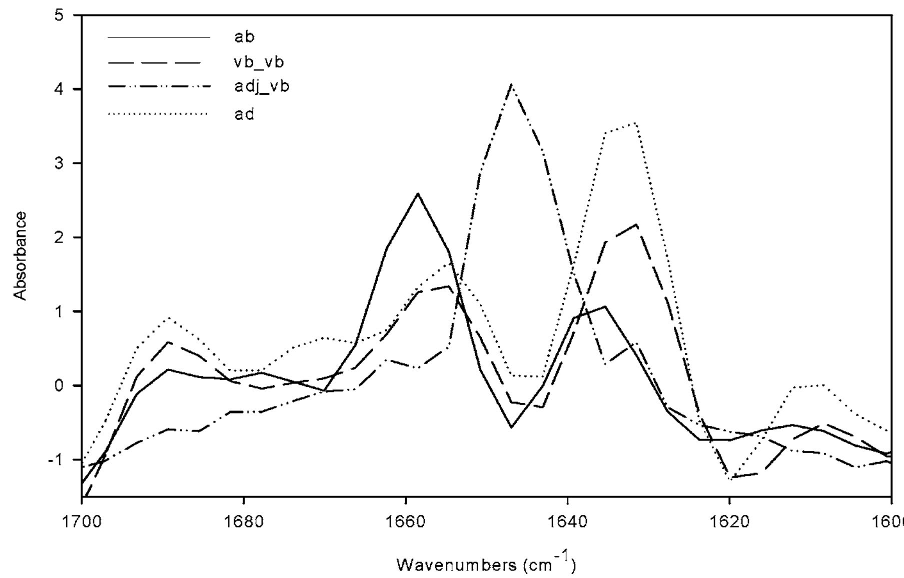

Figure 6. Fourier self-deconvolved spectra of amide I peak from different parts of cotyledon. ab, abaxial; vb_vb, between vascular bundles; adjvb, adjacent to vascular bundle; ad, adaxial.

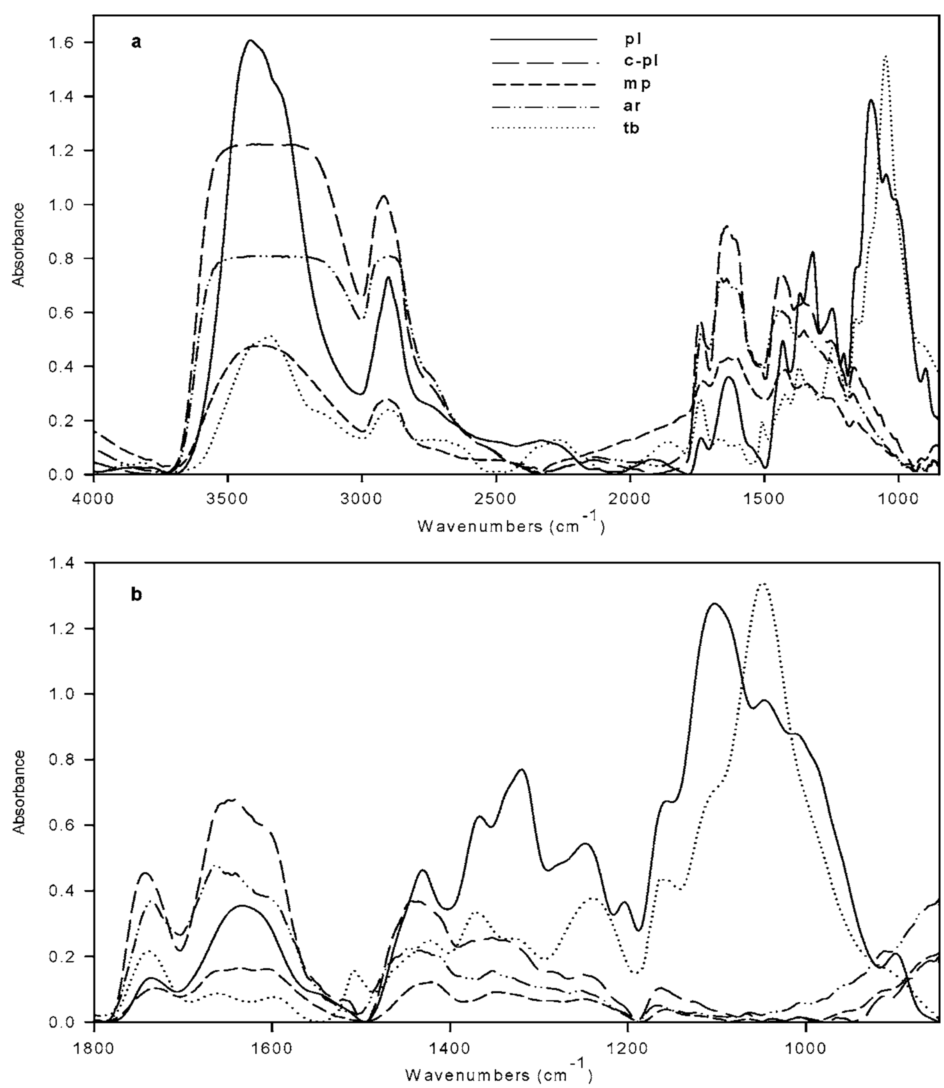

Figure 7. Spectra from different parts of hilum region: (**a**) spectral range 4000–900 cm^{-1}; (**b**) spectral range 1800–900 cm^{-1}. pl, palisade layer; c-pl, counter palisade layer; mp, modified parenchyma; ar, aril; tb, tracheid bar.

expanded in **Figure 7b**. Lipids appear to be present in all tissues, but the palisade layer and tracheid bar contain, as expected, the lowest amount; there is also very little protein in these tissues. No amide I signal was detected in the tracheid bar,

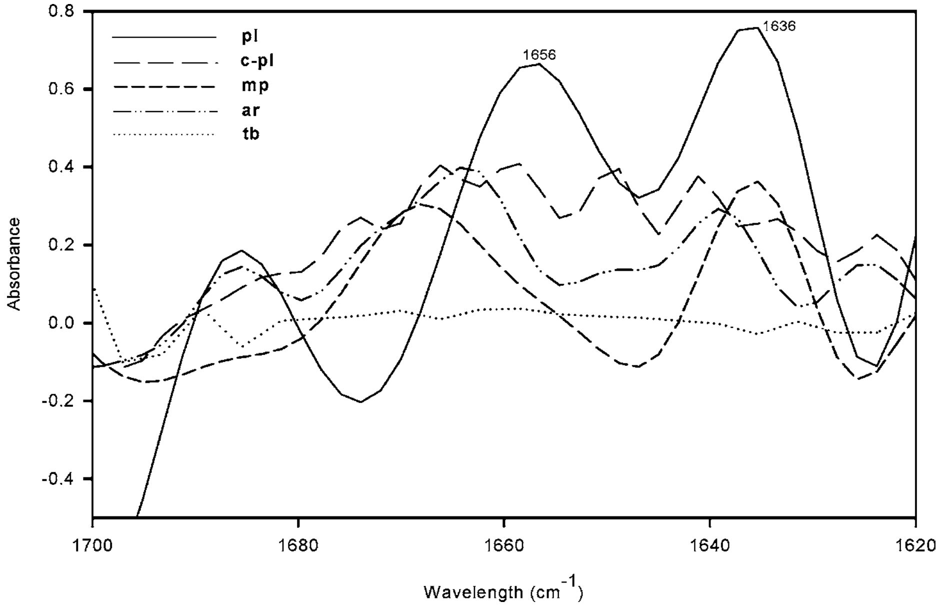

Figure 8. Fourier self-deconvolved spectra of amide I peak from different parts of hilum. pl, palisade layer; c-pl, counter palisade layer; mp, modified parenchyma; ar, aril; tb, tracheid bar.

although a small peak of amide II (1550 cm^{-1}) was present. This peak was not observed in any other hilum tissue, where proteins are represented by the amide I peak only (1656 cm^{-1}). The highest concentrations of protein were observed in the counterpalisade layer, modified parenchyma, and aril. The amide II band at 1550 cm^{-1} is almost nonexistent, particularly in the palisade layer. The counterpalisade layer, modified parenchyma, and aril contain relatively high amounts of lipids and proteins (represented by the amide I band at 1650 cm^{-1}), in comparison with the tracheid bar and palisade layer.

The hilum area shows very high diversity in carbohydrate content measured in the region from 1200 to 1000 cm^{-1}. The tracheid bar, which is a specialized vascular structure, is characterized by a clear band at 1050 cm^{-1} and a shoulder at 1100 cm^{-1}, indicating the presence of cellulose. The tracheoid cells are typically oriented perpendicular to the hilar groove, with walls that are lignified and heavily pitted (*15*). In the spectra from the aril, counterpalisade, and modified parenchyma, the 1450−1325 cm^{-1} region shows significant absorption that can be attributed to hemicellulose and cellulose (**Figure 7b**). The amount of carbohydrate in the palisade layer is relatively high. This layer shows an additional well-developed band, probably of cellulosic origin, at 1100 cm^{-1}. The considerable heterogeneity and diversity of the tissues in the hilum area are most likely a reflection of their morphological and physiological functions as well as different patterns of development (*11*). The high concentration of carbohydrates in this region may play a substantial role in the regulation of seed water absorption.

FTIR self-deconvolution indicates that the molecular configuration of the proteins differs in the different cell types of the hilum (**Figure 8**). The counterpalisade layer and aril contain mainly α-helix and β-sheet structures, but the modified parenchyma also shows some aggregated strands of antiparallel β-sheet.

In conclusion, we have shown that FTIR microspectroscopy using synchrotron radiation is a powerful tool to explore the chemical components of the soybean seed in situ. Differences in the nature and distribution of proteins, lipids, and carbohydrates across the cotyledon and in the hilum region have been demonstrated. It has also been found that these components are not evenly distributed within the cotyledon, but form clusters. The pattern of protein distribution in the cotyledon is very similar to the distribution of water during imbibition. Using this type of characterization, we will ultimately gain a better understanding of the physiological processes in the seed, as well as the physicochemical basis of quality traits that are currently measured by more empirical tests.

ACKNOWLEDGMENT

We gratefully acknowledge the hospitality of the National Synchrotron Light Source at Brookhaven National Laboratory. We thank Fred Wong for the excellent drawings of soybean anatomy, as well as Lisa Miller and Neb Marinkovic at Brookhaven and David Wetzel at Kansas State University for many helpful discussions.

LITERATURE CITED

(1) Pietrzak, L. N.; Fregeau-Reid, J.; Chatson, B.; Blackwell, B. Observations on water distribution in soybean seed during hydration processes using nuclear magnetic resonance imaging. *Can. J. Plant Sci.* **2002**, *82*, 513−519.

(2) Wolf, B. D.; Cowan, J. C. *Soybean as a Food Source*; Chemical Rubber Publishing: Cleveland, OH, 1971; p 17.

(3) Aspinall, G. O.; Begbie, R.; McKay, J. E. Polysaccharide components of soybeans. *Cereal Sci. Today* **1967**, *12* (6), 24−29.

(4) Carr, G. L.; Williams, J. P. Infrared microscopy with synchrotron radiation. In *Accelerator-Based Infrared Sources and Applications*; SPIE Conference Proceedings; Society of Photographic Instrumentation Engineers: Redondo Beach, CA, 1997; Vol. 3153, p 51.

(5) Reffner, J. A. Instrumental factors in infrared microspectroscopy. *Cell. Mol. Biol.* **1998**, *44*, 1−7.

(6) Carr, G. L. Resolution limits for infrared microspectroscopy explored with synchrotron radiation. *Rev. Sci. Instrum.* **2001**, *72*, 1613−1619.

(7) Miller, L. M.; Tague, T. J. Development of biomedical applications of fluorescence-assisted synchrotron infrared microscopy. *Vib. Spectrosc.* **2002**, *849*, 1−7.

(8) Dumas, P. Microanalysis and imaging capabilities of synchrotron infrared microscopy. *J. Phys. IV* **2003**, *104*, 359−364.

(9) Kauppinen, J. K.; Moffat, D. J.; Mantsch, H. H.; Cameron, D. G. Resolution enhancement of amide I peak in FTIR spectrum. *Appl. Spectrosc.* **1981**, *35*, 271−276.

(10) Wetzel, D. L.; Eilert, A. J.; Pietrzak, L. N.; Miller, S. S.; Sweat, J. A. Ultraspatially-resolved synchrotron infrared microspectroscopy on plant tissue *in situ*. *Cell. Mol. Biol.* **1998**, *44*, 145−167.

(11) Miller, S. S.; Bowman, L.-A.; Gijzen, M.; Miki, B. L. A. Early development of the seed coat of soybean (*Glycine max*). *Ann. Bot.* **1999**, *84*, 297−304.

(12) Surewicz, W. K.; Mantsch, H. H. New insight into protein secondary structure from resolution enhanced infrared spectra. *Biochim. Biophys. Acta* **1988**, *952*, 115−130.

(13) Surewicz, W. K.; Mantsch, H. H.; Chapman, D. Determination of protein secondary structure by Fourier transform infrared spectroscopy: a critical assessment. *Biochemistry* **1993**, *32*, 389−394.

(14) Ma, Ch.-Y.; Rout, M. K.; Mock, W.-Y. Study of oat globulin conformation by Fourier transform infrared spectroscopy. *J. Agric. Food Chem.* **2001**, *49*, 3328−3334.

(15) Werker, E. *Seed Anatomy*; Gebrüder Borntraeger: Berlin, Germany, 1997; pp 84−149.

(16) Heil, J. R.; McCarthy, M. J.; Ozligen, M. Magnetic resonance imaging and modeling of water up-take into dry beans. *Lebensm. Wiss. -Technol.* **1992**, *12*, 280−285.

Received for review March 17, 2005. Revised manuscript received July 5, 2005. Accepted September 22, 2005. The generous financial support of Canadian Light Source Inc. is gratefully acknowledged.

JF050608X